

RESEARCH ARTICLE

# The heterogeneity of lithofacies types, combination modes, and sedimentary model of lacustrine shale restricted by high-frequency sequence

Biao Sun<sup>1,2</sup> | Xiaoping Liu<sup>1,2</sup> | Jie Liu<sup>3</sup> | Gaocheng Wang<sup>4</sup> | Honglin Shu<sup>4</sup> |  
Yufeng Luo<sup>4</sup> | Tian Liu<sup>1,2</sup> | Zuxian Hua<sup>1,2</sup>

<sup>1</sup>State Key Laboratory of Petroleum Resources and Prospecting, China University of Petroleum (Beijing), Beijing, China

<sup>2</sup>College of Geosciences, China University of Petroleum (Beijing), Beijing, China

<sup>3</sup>Sinopec International Petroleum Exploration and Production Corporation, Beijing, China

<sup>4</sup>Research Institute of Petroleum Exploration Development, PetroChina Zhejiang Oilfield Company, Hangzhou, China

## Correspondence

Xiaoping Liu, College of Geosciences, China University of Petroleum (Beijing), Beijing 102249, China.  
Email: liuxiaoping@cup.edu.cn

## Funding information

National Natural Science Foundation of China, Grant/Award Number: 42072150

Handling Editor: Z.-Q. Chen

The second Member of the Funing Formation in the Haian Sag of the Subei Basin is a set of organic-rich fine-grained sedimentary rocks, which is a key interval for shale oil exploration. Under the premise of establishing a high-frequency sequence framework, the fine description of the lithofacies change characteristics of the continental fine-grained sedimentary rocks is the basis for the prediction of shale oil favourable areas and the optimization of the production horizons. This study is established through wavelet transformation of the natural gamma curve of the high-frequency sequence framework of the second Member of the Funing Formation, using thin-section observation, total organic carbon analysis, and X-ray diffraction experiments to study the lithofacies types and characteristics of fine-grained sedimentary rocks, and discuss the combination of lithofacies under the high-frequency sequence framework Mode and influencing factors. The results show that the second Member of Funing Formation is composed of three-level sequence of low-level system tract (LST), transgressive system tract (TST), and early high-level system tract (EHST), corresponding to 6 fourth-level sequences and 10 fifth-level sequences. According to the division scheme of “abundance of organic matter + mineral composition + sedimentary structure”, it is found that 12 types of lithofacies were developed in the fine-grained sedimentary rocks of the second Member of Funing Formation. The lithofacies type is affected by the palaeoenvironment. The organic matter facies are mainly controlled by palaeo-water depth and palaeo-redox conditions, the components are mainly controlled by palaeo-water depth and palaeo-salinity, and the tectonic facies are mainly controlled by palaeo-redox and palaeo-salinity. The lithofacies are regularly superimposed in the high-frequency sequence framework, and three combination modes of A, B, and C are developed. Among them, the type A lithofacies are developed in the low-stand system tract, and the type B lithofacies are developed in the transgressive system. The C-type lithofacies assemblage developed near the largest flooding surface and the early highstand system tract, and combined with palaeoenvironment analysis to establish a lithofacies sedimentary model.

## KEYWORDS

fine-grained sedimentary rock, high-frequency sequence, lithofacies combination, palaeoenvironment, sedimentary model

## 1 | INTRODUCTION

With the development of reservoir characterization and special mining techniques, the characteristics of fine-grained sedimentary rocks as reservoirs have been revealed, and their huge oil and gas resource potential has been confirmed. Therefore, fine-grained sedimentary rocks, especially organic-rich shales with integrated source and storage rock has received increasing attention from industry and academia (Aplin & Macquaker, 2011; Bechtel et al., 2012; Birdwell & Washburn, 2015; Liu et al., 2020; Mussa, Kalkreuth, Pimentel Mizusaki, & Bicca, 2021). Fine-grained sedimentary rock refers to clay-grade and silt-grade sediments (particle size less than 65  $\mu\text{m}$ ). Usually contains mudstone, shale, argillaceous siltstone, and siltstone (Bechtel et al., 2012; Cichon-Pupienis et al., 2021; Li & Schieber, 2018; Ross & Bustin, 2008; Trabuco-Alexandre, Dirkx, Veld, Klaver, & De Boer, 2012). Lithofacies research is one of the important methods for restoring ancient water depth, palaeoclimate, and reconstructing palaeogeographic environment. In addition, the lithofacies type is also a key factor that determines the reservoir properties and completion quality in shale oil exploration and development (Bhattacharya, Carr, & Pal, 2016; Dong, Harris, Ayranci, Twemlow, & Nassichuk, 2015; Ibad & Padmanabhan, 2022; Khalifa, 2005). The most widely used early classification scheme for lithofacies type research is the three-unit graphical method based on mineral composition. However, this type of lithofacies classification scheme has the limitation of a single division factor. With the in-depth study of fine-grained sedimentology and unconventional oil and gas for the needs of exploration, the lithofacies classification scheme has gradually developed towards multiple factors (Chen et al., 2020; Hickey & Henk, 2007; Kai-xun et al., 2016; Ross & Bustin, 2008; Zhang & Li, 2018). At present, the most mainstream is the study of fine-grained sedimentary rocks based on organic matter content, mineral composition, and micro-sedimentary structure. At present, for source rock evaluation and reservoir evaluation for shale oil exploration and development, some scholars have studied the pore characteristics and geochemical characteristics of the Second Member of the Funing Formation, but the lithofacies and its depositional environment have not been studied, which restricts the optimal selection of favourable areas for the Second Member of the Funing Formation (Liu et al., 2020).

Marine fine-grained sedimentary rock deposits are generally considered to be controlled by sea level. In the sequence framework, fine-grained sediments often develop in the transgressive system tract (TST) or the early highstand system tract (LHST) and have different differences in different system tracts. The lithofacies characteristics (Cather et al., 2021; Lapidus, Kerimov, Mustaev, Movsumzade, & Zakharchenko, 2018; Leven, 2013; Nwaezeapu et al., 2018; Zhang, Bai, Jin, & Wang, 2016). Hemmesch, Harris, Mnich, and Selby (2014) studied the distribution characteristics of the minerals and lithofacies of the Woodford Shale in the Permian Basin and found that the high stand system tract (HST) developed mudstone and carbonate interbeds, and the TST developed organic-rich shale (Hemmesch et al., 2014). Chen et al. (2015) found that the TST of fine-grained

sedimentary rocks of the Silurian Longmaxi Formation in the Sichuan Basin developed in-situ graptolite-rich shale and siliceous shale, and the high-stand system tract (HST) developed graptolite-rich shale and calcareous shale, etc. (Chen et al., 2015). The continental fine-grained sediments are often controlled by palaeoclimate, provenance, and relative lake level, and are less affected by tectonic cycles and sudden events. In the sequence framework, fine-grained sediments usually change according to the Milankovitch cycle. And produce periodic laws. The Milankovitch cycle theory was proposed by the Yugoslav scholar Milankovitch. It refers to the periodic changes in sunlight caused by the changes in the orbit of the earth's revolution and rotation, and the periodic changes in sunlight will cause palaeoclimate, weathering, and relative lake level. Periodic changes, so that sediments produce a cyclical record in the formation (Shi, Jin, Liu, & Huang, 2020). Therefore, high-frequency sequence research is very important in terrestrial fine-grained sedimentology, but fine-grained sedimentary rocks often exist as "homogeneous" in conventional sequence stratigraphic studies, based on the termination relationship of seismic reflection and macroscopic heterogeneity of lithology. The method of sequence division is not applicable in the high-frequency sequence division of fine-grained sedimentary rocks (Cao et al., 2019; Shi, Jin, Liu, Zhang, & Huang, 2019; Xuebin et al., 2018).

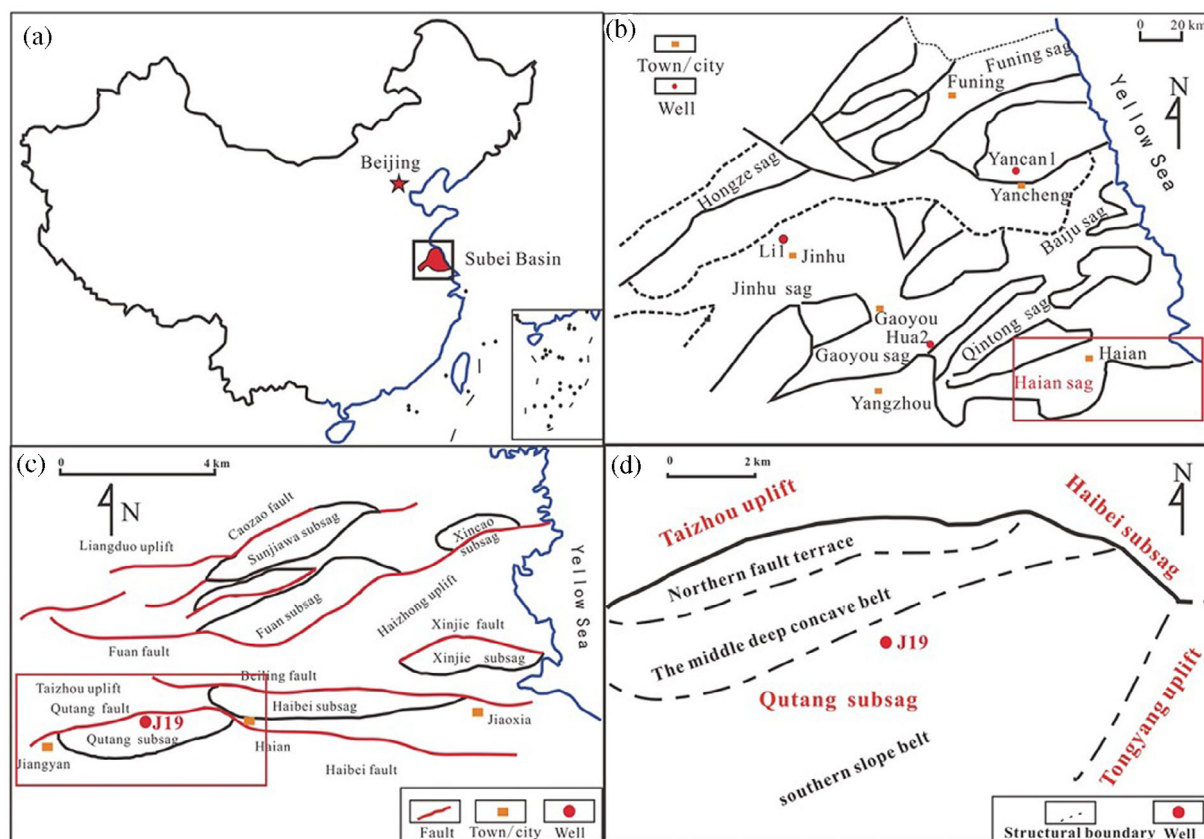
The Funing Formation shale from Subei Basin shows the great potential of shale oil. However, the current research still has the following problems:

1. Predecessors divided the Second Member of the Funing Formation and the Third Member of the Funing Formation into a third-order sequence based on the seismic reflection interface, but the boundaries of the system tract are not clear.
2. There is a lack of research on the lithofacies of the lacustrine fine-grained sedimentary rocks of the Second Member of the Funing Formation.

In this paper, based on its lithological and geochemical characteristics, we formulate a lithofacies classification that is conducive to shale oil exploration. Then, we discuss its lithofacies characteristics and influencing factors in the high-sequence framework.

## 2 | GEOLOGICAL SETTING

The Subei Basin covers an area of about  $3.5 \times 10^4 \text{ km}^2$ , and is the largest Mesozoic–Cenozoic Basin in south-eastern China. It is located between Jiangsu and Anhui Provinces and extends eastward to the Yellow Sea (Figure 1a) (Cheng, Zhang, & Li, 2019; Liu, Lai, et al., 2020), the internal structural units of the basin can be divided into Yanfu Depression, Jianhu Uplift and Dongtai Depression (Figure 1b) (Cheng et al., 2019). The Haian Sag is a secondary structural unit of the Dongtai Depression, located in the south-east of the Subei Basin (Figure 1c). The Qutang sub-sag in the study area is located in the south-western part of the Haian Sag (Figure 1d). It is a pan-shaped fault depression formed in the Late Cretaceous. It has experienced



**FIGURE 1** Location and tectonic units of the study area in Subei Basin. (a) Location of Subei Basin (Liu, Lai, et al., 2020); (b) Division of Basic Structural Units of Subei Basin (Cheng et al., 2019; X. Liu, Lai, et al., 2020); (c) Haian Depression structural unit division (Hu et al., 2018); (d) Qutang sub-sag palaeostructural location map.

two tectonic evolution stages: an early fault period and a late fault period (Wei, Zhang, Liang, Yao, & Tang, 2012; Zhu, Jiang, Xu, & Zhang, 2005). The Qutang sub-sag covers an area of about 430 km<sup>2</sup>. It is adjacent to the Taizhou Low Uplift in the north, Tongyang Uplift in the south, and the Haibei Sub-sag in the east. The overall characteristic is that the north is deep in the south and the north is in the south and the south is overtaken. The northern part of the sub-sag is bounded by the Qutang Fault. From north to south, the northern faulted step belt, the central deep depression area, and the adjacent depression area develop. The southern slope zone and the structural high part of the south-east part of the depression are strong. The internal faults of the depression are strong, and the north-east and north-west directions are developed. There are three groups of faults in the direction and near the east-west direction and the north-east-trending extensional syngenetic faults control the distribution of sediments and sedimentary facies belts in the area (Figure 1d).

The Qutang sub-sag developed four sets of formations, Taizhou, Funing, Dainan, and Sanduo formations from bottom to top. Affected by the Wubao movement, Zhenwu movement, and Sanduo movement, the upper Cretaceous of the Qutang sub-sag. The Eocene is divided into 3 secondary sequences, namely TS<sub>1</sub>, TS<sub>2</sub>, and TS<sub>3</sub>. There are 7 tertiary sequences developed in the secondary sequence framework, which are SQ<sub>1</sub> (K<sub>2</sub>t) and SQ<sub>2</sub>, SQ<sub>3</sub>, SQ<sub>4</sub>, SQ<sub>5</sub>, SQ<sub>6</sub>, and SQ<sub>7</sub>. From bottom to top, the Funing Formation can be subdivided into

four parts. The first Member and the third Member are the delta front and coastal-shallow lacustrine facies deposits are mostly coarse-grained. The Second Member of the Funing Formation and the Fourth Member of the Funing Formation are deep lake-semi-deep lake deposits. The lithology is mainly dark mudstone/shale, with fine-grained sedimentary rocks developed (Figure 2). Although the Funing Formation in the Subei Basin has a continental sedimentary background as a whole, it has been discovered through the study of lithofacies palaeogeography, palaeontology, petrology, and geochemistry that the Second Member of the Funing Formation and the Fourth Member of the Funing Formation are subject to transgression (Fu, Li, Zhang, & Liu, 2008; Wang & Chen, 1992). Therefore, the Second Member of the Funing Formation formed a set of fine-grained sediments of transgressive lake facies under the combined action of transgression and lakes (Fu et al., 2008; Wang & Chen, 1992).

### 3 | EXPERIMENTS AND METHODS

#### 3.1 | Experiments

There is a total of 10 coring times in the Second Member of the Funing Formation of J19 well (Finger 1). The length of each coring is 1.09–18 m, and the total core length is 121.47 m. High-density

sampling is performed on the coring section. The sample interval is generally between 1 and 2 m, and the dense sampling interval of some layers is 0.3 m, and a total of 158 samples were collected. A part of all samples were taken to make rock and mineral thin slices. The remaining samples were washed with ionized water, dried, and ground to 200 meshes for corresponding analysis and testing. Seventy samples were selected for the total organic carbon test, 140 samples for X-ray diffraction analysis test, 18 samples to conduct trace element testing. The total organic carbon content (TOC) of the sample was obtained with the LECO CS-230 carbon and sulfur analyser, and the test was carried out by the National Standard for the Determination of Total Organic Carbon in Sedimentary Rocks GB/T 19145-2013. The XL20042174X diffractometer (D453) was used to obtain the mineral composition and content of the sample, and the test was performed according to the national X-ray diffraction analysis standard SY/T 5163-2010 for clay minerals and common non-clay minerals in sedimentary rocks. Trace elements were tested at the Chengdu University of Technology. First, the samples were soaked in acid liquid. Then, the coupled plasma mass spectrometer (ELAN9000) was used to obtain the trace element information of the samples.

### 3.2 | Wavelet analysis

Wavelet transform is a signal processing tool that converts a certain signal into other forms of signals. It can effectively reveal the hidden information in the signal (Kadkhodaie & Rezaee, 2017). Its principle is based on the Fourier transform, using a certain proportion and period. The mother wavelets are used to process the time series signal to obtain a series of wavelet coefficients corresponding to the ratio, to find more hidden information in the time-frequency domain of the non-stationary signal (Chen et al., 2020). Rich geological information is preserved in lacustrine sediments (Olsen & Whiteside, 2009), and its periodic changes can be well represented in logging curves. Logging curves can be regarded as a set of discrete sequences with different frequencies. The depth domain corresponds to the time domain, so discrete wavelet transforms (DWT) can be used for analysis. The independent frequency signals of different frequencies (deposition period) contained in the logging signal are displayed in different scales after DWT, where different scales represent different deposition cycles, and the wavelet coefficient curve oscillation position within the same scale also represents the boundary of the deposition cycle (Trabucho-Alexandre et al., 2012; Tucker & Garland, 2010; Wei et al., 2012).

The main process of wavelet analysis includes (1) Sampling, selecting the natural gamma curve that is sensitive to changes in lake level up and down, and extracting values at equal intervals at a depth of 0.125 m; (2) Signal expansion and signalling to both ends of the discrete series Expand to eliminate the influence of boundary effects and remove the expanded part after DWT; (3) Filter to remove low-frequency and high-frequency interference; (4) DWT to obtain wavelet coefficients of different scales Curves, wavelet coefficient variance curves, and time-frequency chromatograms are used to explore the

periodicity of deposition, to classify the order of the sequence and determine the sequence interface.

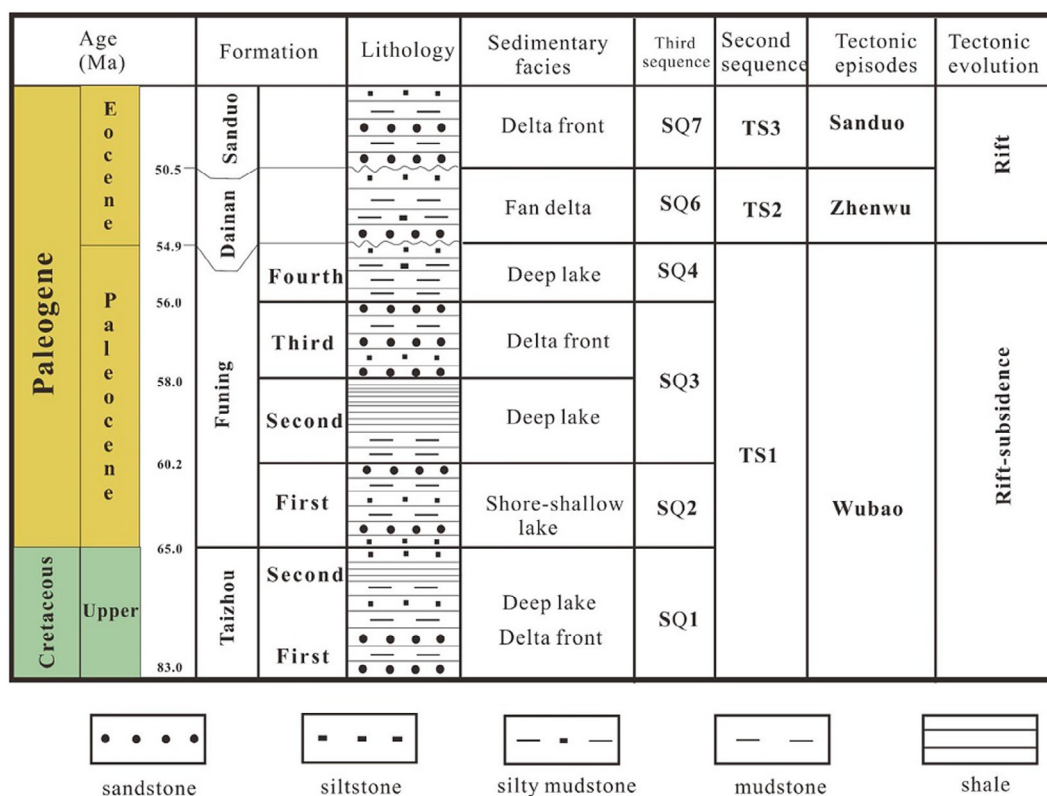
The basic requirement of wavelet transform is that there is no major interruption in the data. The logging data used in this study is continuously sampled at 0.125 m intervals, so DWT can be performed. All data processing in this study was completed in the MATLAB 2020 software wavelet toolbox.

## 4 | RESULTS

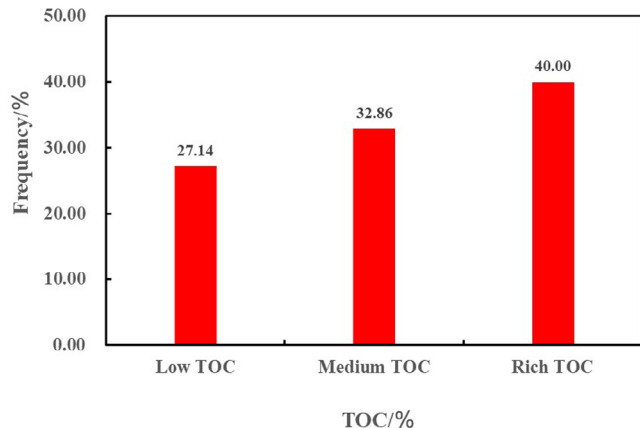
### 4.1 | Organic petrology, sedimentary, and lithofacies division

Lithofacies refers to the types of rocks formed in a specific sedimentary environment. The classification basis mainly includes the abundance of organic matter, mineral composition, and sedimentary structure. Through the analysis and testing of 70 samples from the second section of Funing Formation section, it can be seen that the (TOC) is between 0.20 and 3.22%, with an average of 1.61%. Generally speaking, the TOC of the terrestrial low-mature mud shale has a certain relationship with the hydrogen index (HI). When the TOC is less than 1%, the HI is at a low value, and when the TOC is 1–2%, the HI and TOC are positively correlated. When TOC > 2%, HI tends to be stable and does not increase with the increase of TOC (Dahl et al., 1994; Flemming, 2000; Loucks & Ruppel, 2007; Pepper & Corvi, 1995). Therefore, the shale organic facies in the study area can be divided into organic-rich facies, medium-organic facies, and poor organic facies as the boundary of 1% and 2% The distribution characteristics of the organic matter are shown in Figure 3. According to X-ray diffraction experiments of 140 samples, the main mineral components of the second Member of Funing Formation are clay minerals, carbonate minerals (calcite and dolomite), and felsic minerals (feldspar and quartz). The distribution characteristics are shown in Figure 4. The clay minerals the content is between 0 and 63%, and the average is 35.31%, the felsic mineral content is between 5 and 50%, and the average is 30.48%, and the carbonate mineral content is between 1 and 72%, and the average is 27.46%. It also contains a small amount of analcime, pyrite, etc. On the whole, the content of the main minerals in the second Member of Funing Formation is relatively even, and the dominant minerals are not obvious. According to the normalization results of the main minerals, the fine-grained rock is divided into clayey fine-grained rock, carbonate fine-grained rock, felsic fine-grained rock, and mixed fine-grained rock, among which mixed fine-grained rock can be fine-grained. It is transformed into clay-rich mixed fine-grained rock, carbonate-rich mixed fine-grained rock, and rich felsic mixed fine-grained rock. In fine-grained rocks, the common types of sedimentary structures include laminar (single layer <1 mm), layered (1 mm <single layer <10 mm) and massive (single layer >10 mm). Observation under the thin-film microscope shows that the fine-grained rock of the section is mainly in block, layer, and laminar shape, and the specific characteristics are shown in Figure 5. According to the above petrological and geochemical characteristics, the lithofacies





**FIGURE 2** Stratigraphic characteristics and sequence stratigraphic framework of the Haian Sag



**FIGURE 3** Distribution of organic matter content in shale of J19 Well, Subei Basin

types are named using “organic matter abundance + mineral composition + sedimentary structure” (Figure 6). The fine-grained sedimentary rock lithofacies of the second Member of the Funing Formation has 12 types. The specific characteristics are shown in Table 1.

## 4.2 | Trace elements

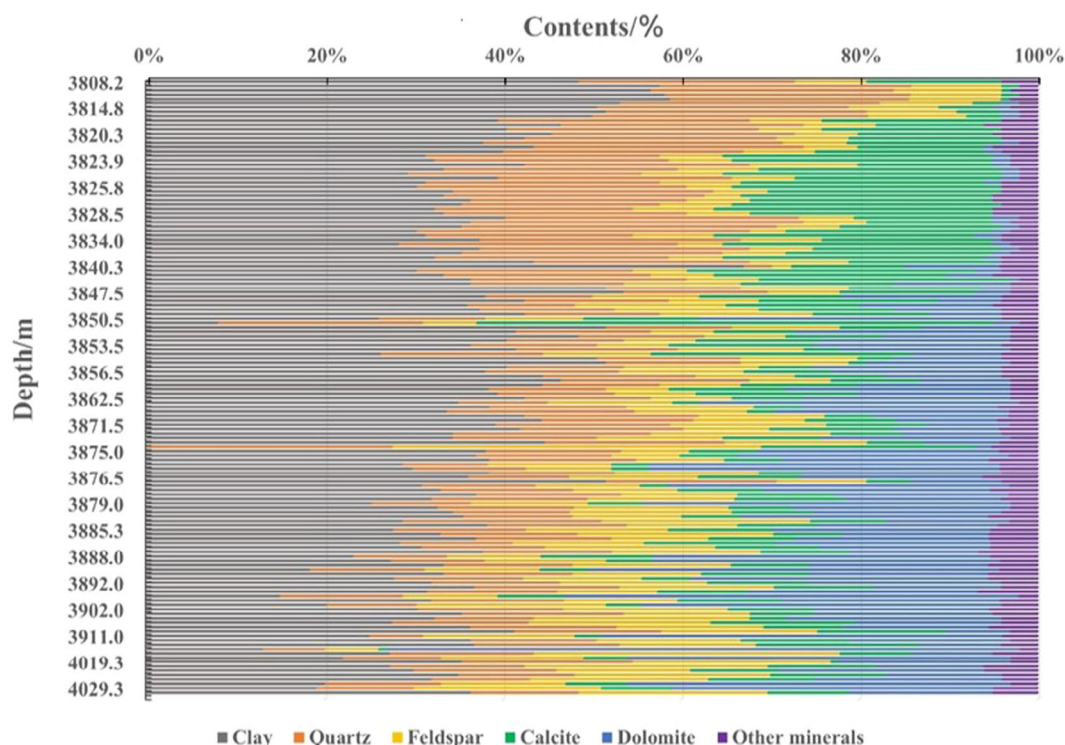
Table 2 lists the contents of trace elements. The average content of V (86.6 mg/kg), Cr (75.1 mg/kg), Sr (556.1 mg/kg), Ba (955.6 mg/kg), Th

(10.7 mg/kg), U (2.3 mg/kg), Co (12.8 mg/kg), Rb (99.2 mg/kg), and Ni (31.6 mg/kg) is greater than 2 mg/kg.

## 4.3 | High-frequency sequence

Using wavelet transform to decompose the GR curve of Well J19 in 10 levels, one approximate curve (a10) and 10 decomposition curves (d1–d10) are obtained (Figure 7). The decomposition curve can enhance the abrupt and fluctuating signal of the natural gamma curve, and the change of the natural gamma value on different scales can be identified through the decomposition curve of different scales, which corresponds to the changes in the lake level of different scales. From the wavelet coefficient variance curve of Well J19, it can be seen that there are three cycles with similar cycles in the second Member of Funing Formation. By comparing the thickness of each cycle with the wave length of GR wavelet decomposition curve of each scale, the wavelet decomposition curve representing each level of cycle can be optimized.

It can be seen from the comparison that the d10, d8, and d7 curve wave lengths correspond well with the thickness of about 100 m (700–800 Ka), 55 m (400–500 Ka), and 35 m (200–300 Ka) formation cycles (Figure 8). It can be used as an effective identification boundary for all levels of sequence or system domain. In the third-order sequence (SQ3) of the second Member and the third Member of the Funing Formation, the early low system tract



**FIGURE 4** Whole-rock mineral component of shale in J19 Well, Subei Basin



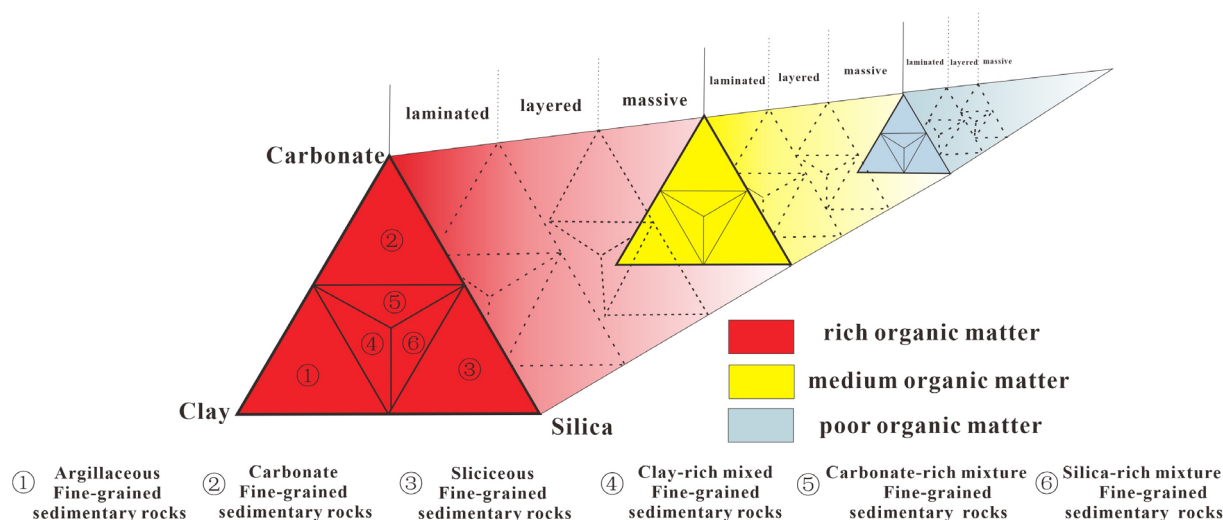
**FIGURE 5** Major sedimentary structure types of the shale in plane-polarized light. a and b: laminated structure (<1 mm); c and d: bedded structure (1 cm >> 1 mm); e and f: massive structure

(LST), the TST, and the early highstand system tract (EHST) developed in the second Member of the Funing Formation, corresponding to 6 Four-level sequence (SQ3-1, SQ3-2, SQ3-3, SQ3-4, SQ3-5, SQ3-6) and 10 five-level sequences (SQ3-1-1, SQ3-2-1, SQ3-2-2, SQ3-3-1, SQ3-3-2, SQ3-4-1, SQ3-4-2, SQ3-5-1, SQ3-5-2, SQ3-6) (Figure 8).

#### 4.4 | Controls of palaeoenvironment on lithofacies


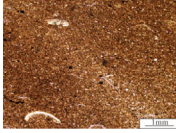
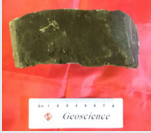
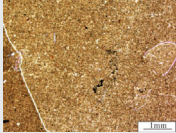

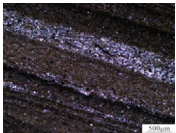

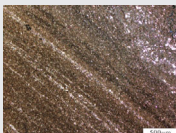

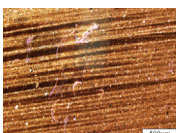

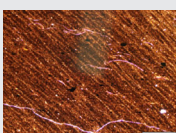

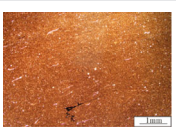
##### 4.4.1 | Palaeoenvironment analysis

The ancient water depth of the lake Basin is usually recovered by the V/Cr and Th/U element ratio method, and when the ratio of V/Cr to



**FIGURE 6** The lithofacies classification scheme of the shale

**TABLE 1** Lithofacies types and characteristics of shale in the Subei Basin

Number	Type	Cores	Thin section	TOC	Mineral composition		
					Clay minerals	Siliceous minerals	Calcareous minerals
1	Organic-rich massive argillaceous facies			$\frac{2.04-2.29}{2.16}$	$\frac{51.0-57.0}{55.6}$	$\frac{36.0-39.0}{37.8}$	$\frac{1.0-7.0}{2.6}$
2	Organic-medium massive argillaceous facies			$\frac{1.30-1.64}{1.47}$	$\frac{50.0-51.0}{50.5}$	$\frac{29.0-42.0}{35.5}$	$\frac{6.0-16.0}{11.0}$
3	Organic-medium laminated carbonate facies			$\frac{1.04-1.60}{1.32}$	$\frac{8.0-22.0}{15.0}$	$\frac{20.0-29.0}{24.5}$	$\frac{48.0-61.0}{54.5}$
4	Organic-poor bedded carbonate facies			$\frac{0.49-0.70}{0.59}$	$\frac{8.0-21.0}{14.7}$	$\frac{19.0-27.0}{23.6}$	$\frac{50.0-61.0}{55.4}$
5	Organic-rich laminated clay-rich mixed facies			$\frac{2.25-3.16}{2.55}$	$\frac{32.0-45.0}{38.7}$	$\frac{28.0-37.0}{33.3}$	$\frac{15.0-31.0}{23.3}$
6	Organic-rich massive clay-rich mixed facies			$\frac{2.02-2.57}{2.29}$	$\frac{31.0-46.0}{37.7}$	$\frac{29.0-35.0}{32.0}$	$\frac{12.0-32.0}{24.7}$
7	Organic-medium massive clay-rich mixed facies			$\frac{1.02-1.41}{1.20}$	$\frac{31.0-42.0}{38.7}$	$\frac{21.0-38.0}{31.8}$	$\frac{20.0-35.0}{27.0}$

(Continues)

TABLE 1 (Continued)


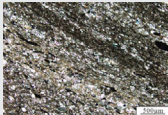

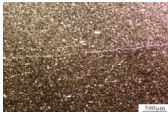

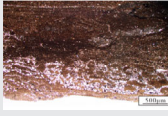

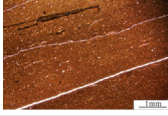

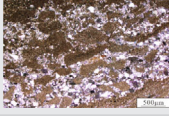
Number	Type	Cores	Thin section	TOC	Mineral composition		
					Clay minerals	Siliceous minerals	Calcareous minerals
8	Organic-medium laminated carbonate-rich mixed facies			$\frac{1.29-1.90}{1.60}$	$\frac{30.0-31.0}{30.5}$	$\frac{30.0-31.0}{30.5}$	$\frac{32.0-33.0}{32.5}$
9	Organic-medium massive carbonate-rich mixed facies			$\frac{1.01-1.10}{1.06}$	$\frac{20.0-31.0}{27.0}$	$\frac{24.0-32.0}{29.8}$	$\frac{32.0-46.0}{36.0}$
10	Organic-poor massive carbonate-rich mixed facies			$\frac{0.51-0.83}{0.67}$	$\frac{28.0-31.0}{29.5}$	$\frac{23.0-25.0}{24.0}$	$\frac{32.0-33.0}{32.5}$
11	Organic-medium massive carbonate-rich mixed facies			$\frac{1.18-1.19}{1.18}$	$\frac{27.0-35.0}{31.0}$	$\frac{41.0-42.0}{41.5}$	$\frac{20.0-24.0}{22.0}$
12	Organic-poor massive silica-rich mixed facies			$\frac{0.49-0.70}{0.59}$	$\frac{27.0-28.0}{27.5}$	$\frac{32.0-43.0}{37.5}$	$\frac{21.0-27.0}{24.0}$

TABLE 2 Trace element contents data of the E<sub>1</sub>f<sup>2</sup> in J19 well in the Subei Basin

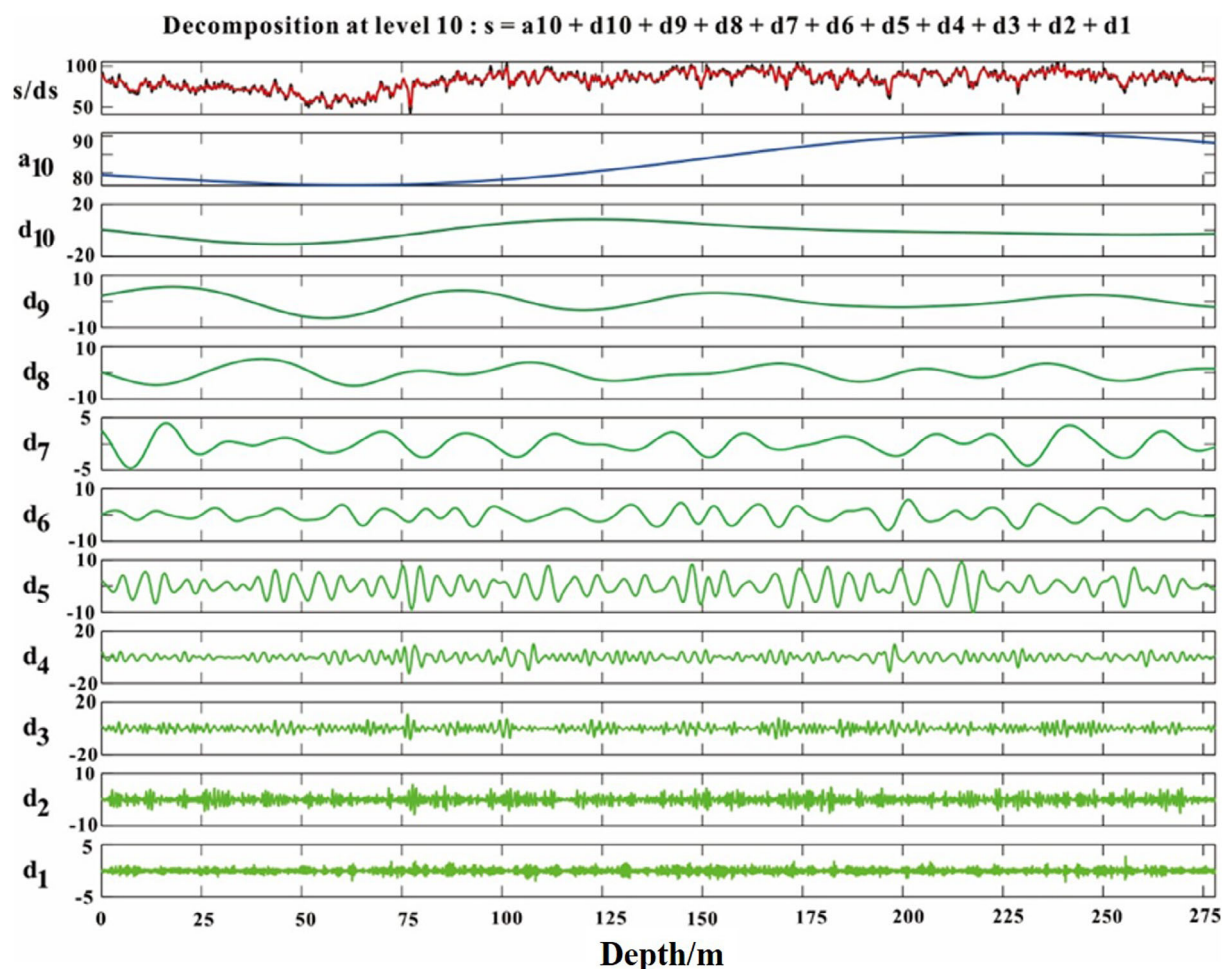
Depth/m	V (mg/kg)	Cr (mg/kg)	Sr (mg/kg)	Ba (mg/kg)	Th (mg/kg)	U (mg/kg)	Co (mg/kg)	Rb (mg/kg)	Ni (mg/kg)
3,811.3	108.7	90.1	193.1	561.9	13.5	2.4	16.2	116.1	42.6
3,814.4	115.8	97.3	204.7	543.3	14.4	2.6	15.3	121.9	41.7
3,820.3	95.2	71.8	286.3	658.7	10.7	2.3	12.2	93.9	29.5
3,829.2	70.0	49.2	587.6	518.4	8.2	1.7	11.1	69.6	24.2
3,830.0	69.7	53.2	358.3	4,566.6	7.5	1.8	11.9	69.2	32.0
3,839.0	65.0	51.2	376.5	579.5	7.6	1.4	11.1	70.1	25.8
3,847.0	103.9	97.5	533.6	721.4	12.7	2.3	13.7	134.1	35.3
3,850.0	100.8	82.3	386.8	718.4	11.1	2.7	14.3	98.7	36.3
3,856.0	112.7	95.2	516.4	661.5	11.7	3.1	15.8	129.1	41.9
3,861.0	84.4	71.1	801.0	477.0	10.8	2.4	13.9	108.0	38.6
3,870.0	80.4	72.5	787.9	1,156.8	10.9	2.2	12.0	106.5	31.4
3,875.5	87.7	75.5	640.1	506.7	9.9	1.8	16.1	102.6	32.1
3,883.0	96.4	97.5	603.4	640.7	10.7	2.0	11.4	113.9	28.1
3,891.3	88.9	86.6	471.7	458.7	9.7	1.8	13.5	109.5	32.2
3,902.0	66.8	64.5	854.8	1,123.5	9.4	2.1	10.8	81.7	23.9
3,905.0	82.9	73.5	537.7	1,098.8	8.6	2.3	11.1	94.2	25.9
3,914.0	50.6	41.7	814.3	1,340.7	11.7	3.0	8.6	68.0	17.9
4,021.3	84.9	80.1	783.7	700.9	12.6	3.0	11.6	89.3	29.5

Th/U is higher, the ancient water is deeper (Jones & Manning, 1994). According to the distribution law, the V/Cr of this sample the ratios all ranged from 0.99 to 1.42, with an average of 1.17. The Th/U ratios all ranged from 3.74 to 5.62, with an average of 4.76. Based on the ancient water depth recovered by the V/Cr and Th/U ratio method,

the water depth of the target zone in the study area has been increasing (Figure 9).

The ancient salinity of lake basins is generally characterized by the Sr/Ba element method, and the principle of ancient salinity recovery using Sr/Ba is based on the characteristics of separation of Sr and





**FIGURE 7** The db wavelet transform of natural gamma curves of the shale of J19 well

Ba elements in different sedimentary environments due to differences in geochemical behaviour (Dymond, 1992; Jarvis, Murphy, & Gale, 2001). According to the statistical results, the Sr/Ba ratios of this sample ranged from 0.08 to 1.68, with an average of 0.76. Considering the characteristics of the Sr/Ba ratio, it can be seen that the target layer, the Haian Sag is a freshwater-saltwater environment, and the freshwater environment is taken as mainly, there are occasional local salt water environments formed by transgressions (Figure 9).

The palaeoclimate of the lake Basin is evaluated by the ratio of Rb/Sr and Sr/Cu (Boucot & Gray, 2001; Yang et al., 2019). The ratio of Sr/Cu in this sample is all between 4.55 and 44.02, with an average of 19.99. The Rb/Sr ratios all ranged from 0.08 to 0.60, with an average of 0.23. Synthesizing the palaeoclimate recovered by the Rb/Sr and Sr/Cu ratio methods, it is found that the second Member of the Funing Formation in the Haian Sag is semi-arid and semi-humid as a whole, and the climate conditions continue to become humid from the bottom to top (Figure 9).

The ancient redox conditions are mainly related to the content of free oxygen in the lake water, and the redox properties of the water are mainly characterized by the ratio of V/(V + Ni), Ni/Co and U/Th elements (Flemming, 2000; Nwaezeapu et al., 2018). The V/(V + Ni)

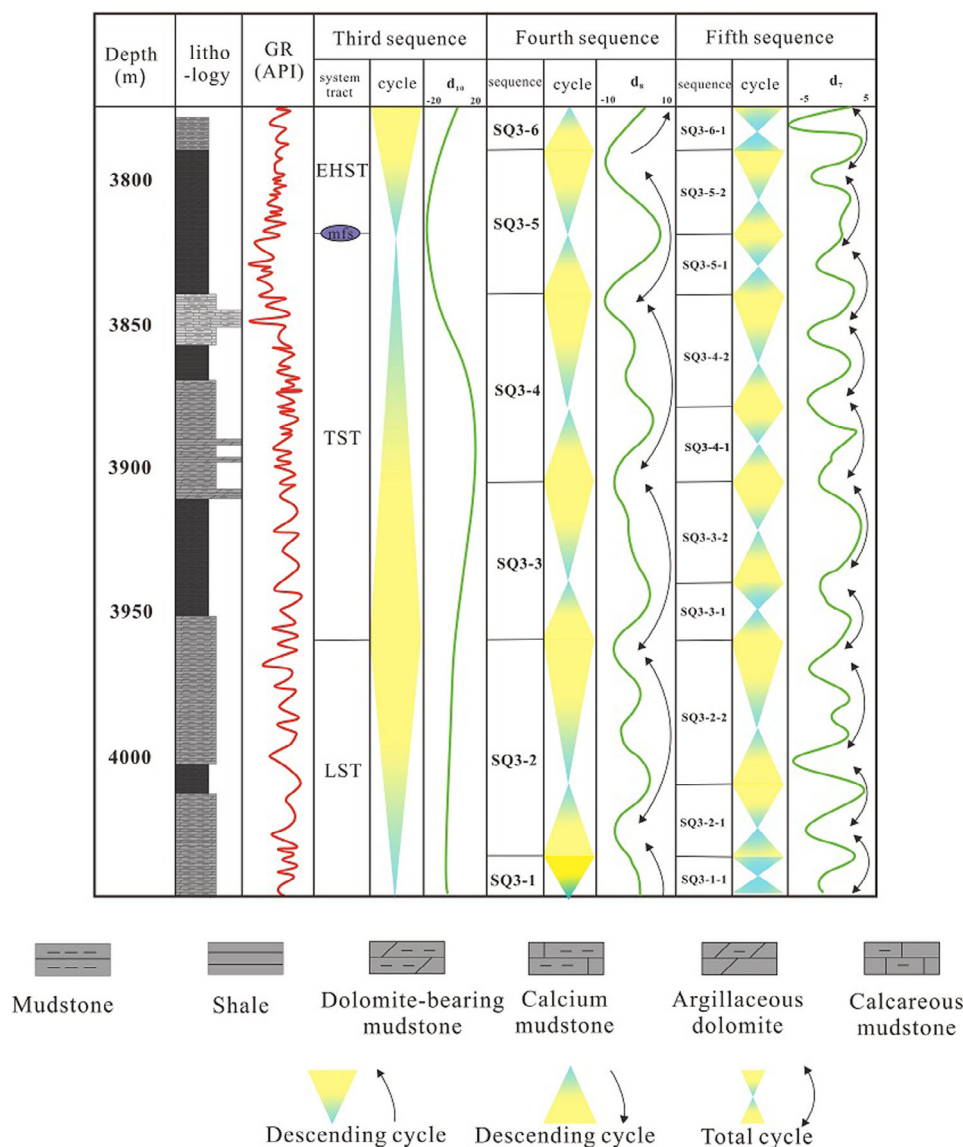
ratios of this sample all ranged from 0.69 to 0.76, with an average of 0.73. The Ni/Co ratios all ranged from 1.99 to 2.78, with an average of 2.45. The U/Th ratios all ranged from 0.18 to 0.27, with an average of 0.21. Based on the palaeo-redox conditions recovered by the ratio of the three methods, it is found that the second Member of the Funing Formation in the Haian Sag is in a semi-reduced-semi-oxidized environment (Figure 9).

On the whole, the environment in the study area is a deep lake, and the water environment gradually deepens vertically; the palaeo-salinity is a freshwater environment, but the vertical palaeo-salinity shows a trend of increasing and then decreasing; the palaeoclimate is semi-arid-semi-humid, which gradually evolves to warm and humid vertically; palaeo redox conditions are semi-reducing-semi-oxidizing environment.

#### 4.4.2 | Influences of palaeoenvironment on lithofacies

The ancient water depth and ancient oxidation conditions affect the productivity and preservation conditions of organic matter to a certain



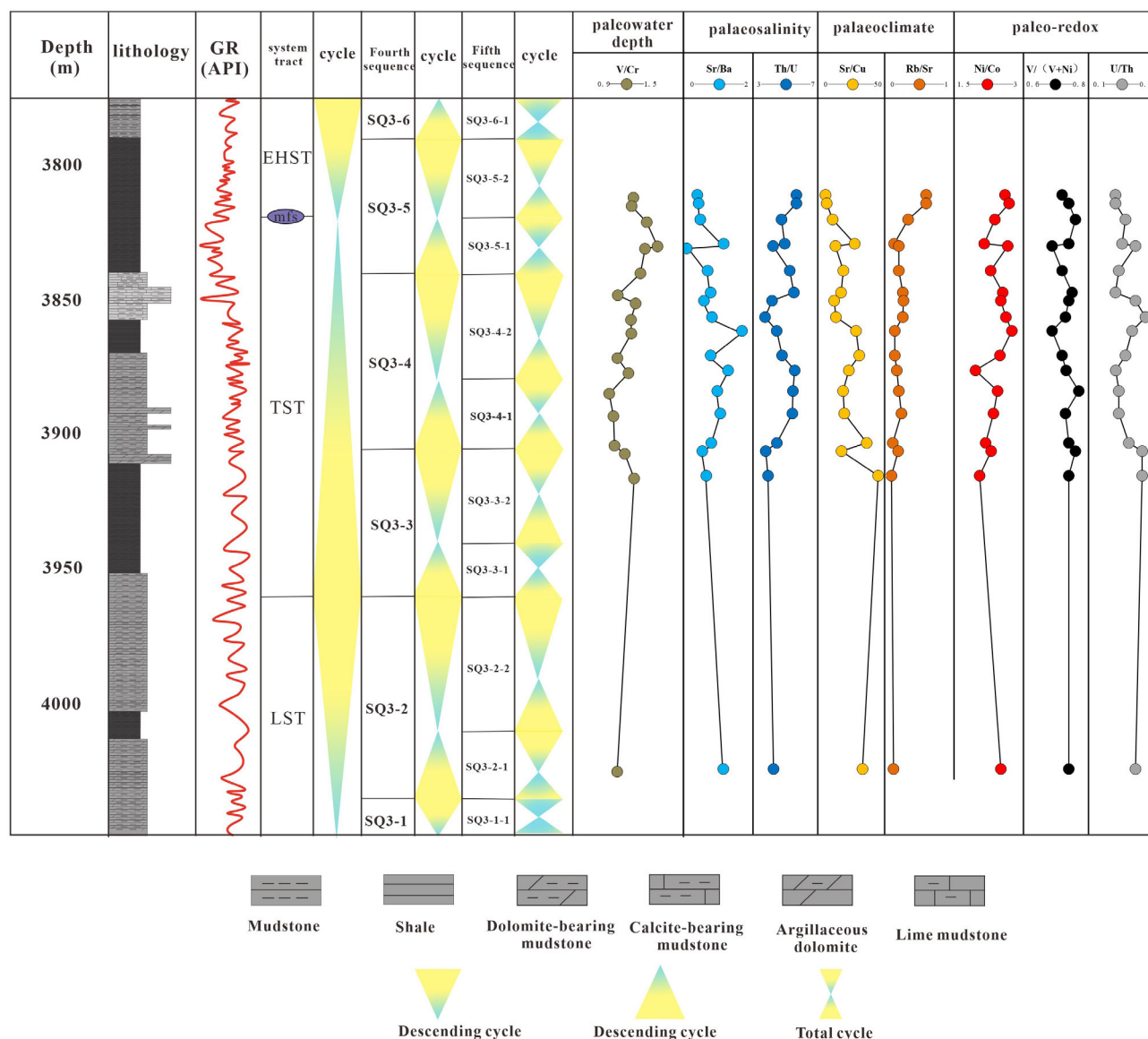


**FIGURE 8** High-frequency stratigraphic sequence based on wavelet analysis of the J19 well

extent, and control the abundance and distribution of organic matter (Figure 10a–d). The redox environment is a key factor affecting the organic carbon content, and it controls the degree of preservation of organic matter. There are many factors in the burial process that will cause the organic matter to be diluted and destroyed. In the hypoxic reduction environment, due to the lack of aerobic biological activity, the organic matter can be well preserved. Therefore, the organic carbon content and the ancient water depth are strongly positive. Correlation (Figure 10a). Areas with high values of organic matter are often located in relatively deep areas of saline water and brackish water (Figure 10b). The enrichment of nutrient elements in saline-brass water lakes will provide a nutritional guarantee for the prosperity of a large number of planktons. Under normal circumstances, saltwater lakes have high productivity, saltwater-brass water lakes are prone to form salinity stratification, and the bottom water body in deep water contains Low oxygen content is often in a reduced state, which is conducive to the preservation of organic matter, and ultimately manifests itself in the same characteristics as the high-value palaeo-salinity area and the organic matter-rich area.

The felsic minerals and clay minerals in the fine-grained sedimentary rocks of the second Member of the Funing Formation are weakly positively correlated with the palaeo-water depth (V/Cr) (Figure 11). The impact cycle (400–500 Ka), can be divided into a half cycle with a dry and cold climate and a half cycle with a warm and humid climate. In the warm and humid half-cycle, rainfall is abundant. The rising of the lake level also enhances the weathering of the land surface, causing more terrestrial debris to enter the lake Basin. Conversely, the dry and cold half-cycle has less rainfall, and the lake level drops and the lake level drops. The weakening of weathering led to the decrease of felsic minerals and clay minerals in the lake Basin.

Carbonate deposition is mainly affected by ancient salinity, and the change of ancient salinity is mainly affected by transgression. On the one hand, the seawater has high salinity and density. When seawater intrudes into the lake water, it is easy to sink, which makes the lake water salty. At the same time, a stagnant water layer is produced, causing slow vertical convection of the lake water, forming a relatively reduced high-salinity environment at the bottom of the lake, and high salinity is a favourable condition for the formation of dolomite; on the



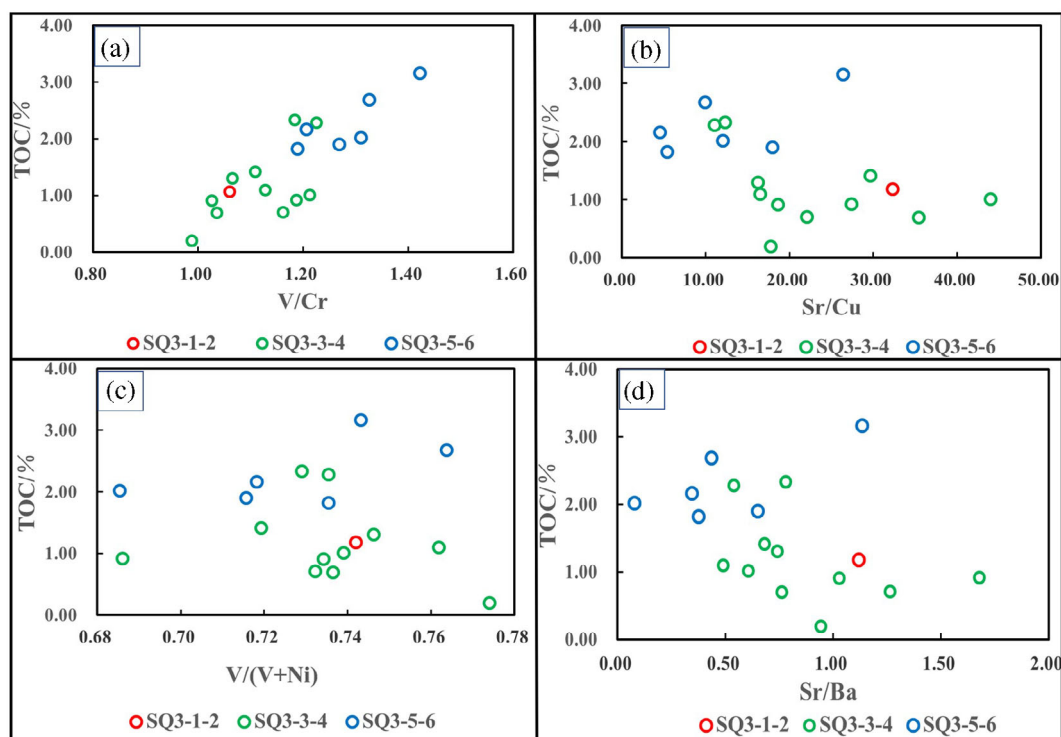
**FIGURE 9** The stratigraphic distribution of the palaeo water (V/Cr), palaeosalinity (Sr/Ba and Th/U), palaeoclimate (Sr/Cu, Rb/Sr, and Ni/Co), palaeo redox conditions (V/(V + Ni) and U/Th) of the J19 well

other hand, the seawater is alkaline. One of the conditions for the formation of dolomite is that it needs a higher pH value (weakly alkaline-alkaline). The intrusion of sea water increases the pH value of the lake water, which is easy to form a weakly alkaline-alkaline reducing environment, which is conducive to dolomitization.

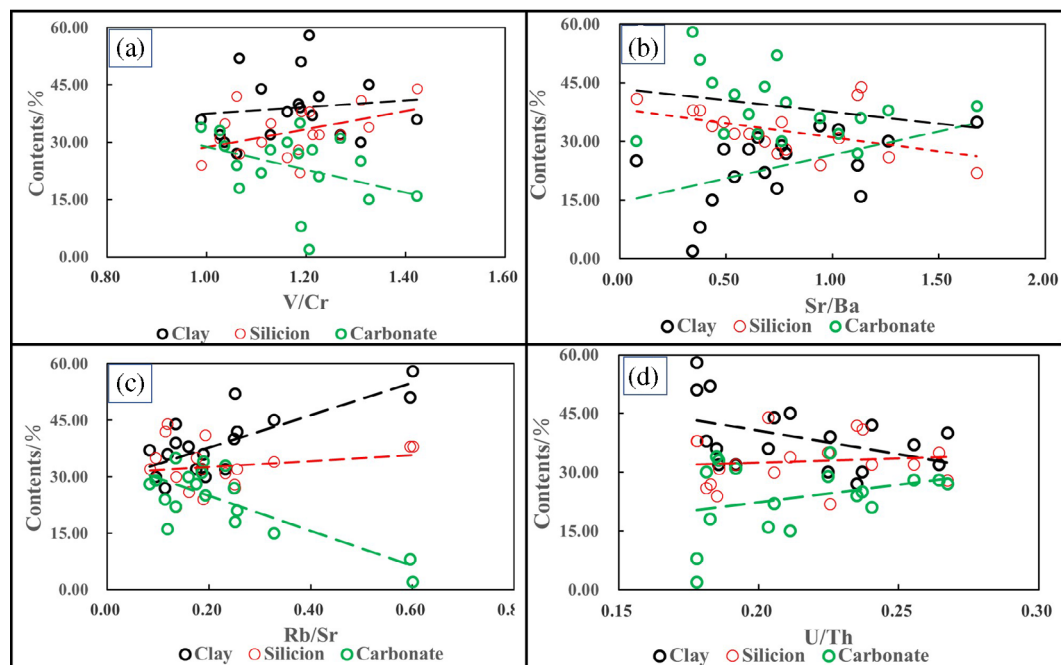
Affected by palaeo-redox properties, the laminae are mainly developed in the reduction zone. The fine-grained sedimentary laminae of the mud shale in the second Member of the Funing Formation of the Haian sag are mainly composed of carbonate laminae and organic-rich muddy laminae. Therefore, the formation of the laminae the first condition is that the carbonate component and argillaceous component are frequently and periodically re-supplied. The shallow lake area is obviously controlled by the provenance of terrigenous clastic. The terrigenous clastic is injected into the lower part of the water with high shale content, the water body is turbid, which is not

conductive to the development of carbonates and the laminae is not developed; the water with low terrigenous clastic input in the lower high part, the water body is clear and the carbonate rock is relatively rich, but the argillaceous content is low, and the laminae are not developed. In the deep lake area, water bodies gather in multiple directions, and the water body has a strong dilution effect (Wang Yong et al., 2016), and carbonate components are not enriched, which is not conducive to the development of laminae (Figure 12).

Palaeo-salinity affects the solubility of the water medium to a certain extent, thereby controlling the sedimentary structure. The carbonate component in the fine-grained mixed rock is mostly the product of the continuous extraction of  $\text{CO}_2$  from algae photosynthesis, which leads to an increase in the concentration of water  $\text{CO}_3^{2-}$  and interacts with the  $\text{Ca}^{2+}$  carried by the lake surface. Under normal circumstances, the high concentration of  $\text{CO}_3^{2-}$  and  $\text{Ca}^{2+}$  ions in



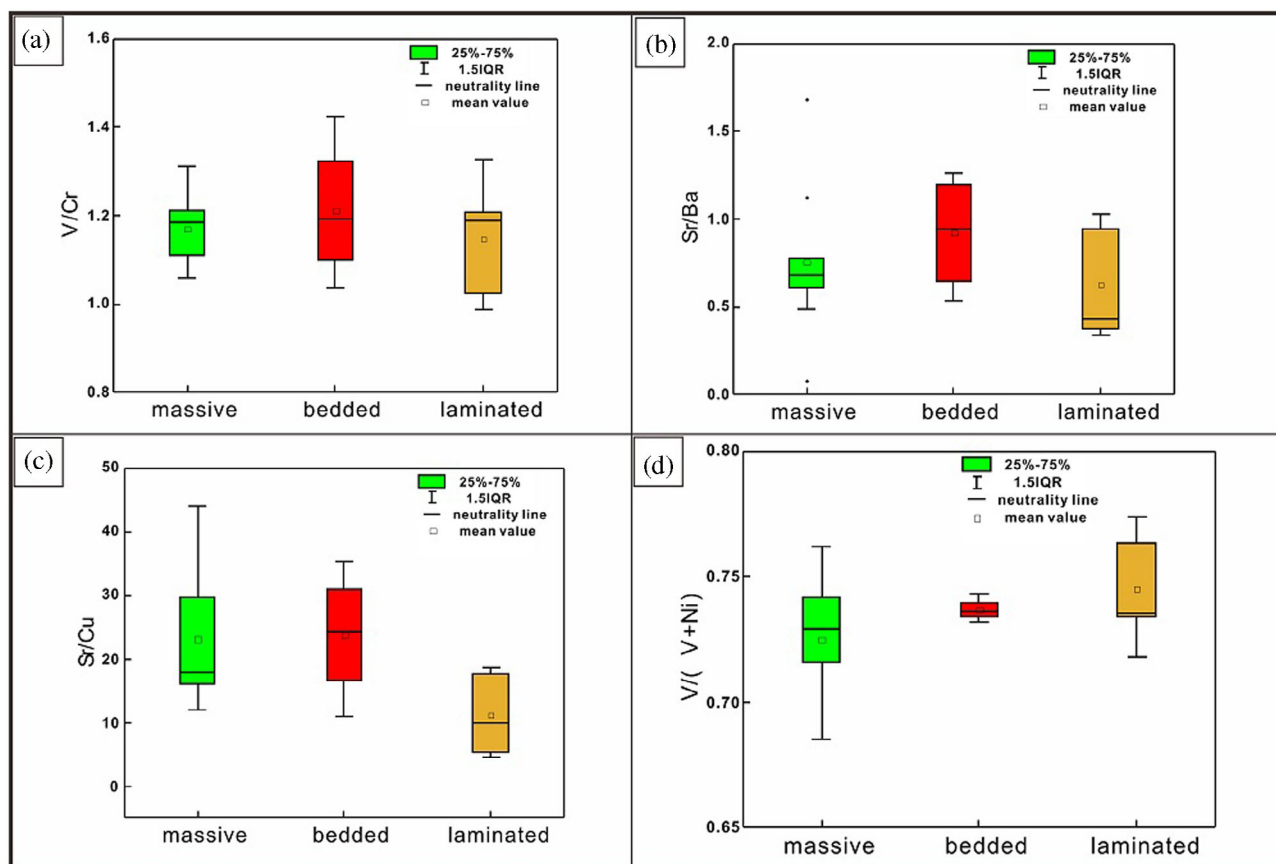
**FIGURE 10** Governing factors of organic matter



**FIGURE 11** Governing factors of mineral components

high-salinity water is conducive to the deposition and precipitation of fine microcrystalline carbonates. The archaea and sulfate-reducing bacteria at the bottom of the salty lake metabolize together (a large number of laminar micro-crystalline carbonate development sections develop the thin layered or massive gypsum rock), which increases

the pH of the water environment, provides conditions for the preservation of carbonate particles at the bottom of the lake. Eventually, carbonates are mostly produced in the form of laminar fine crystals. When the water body deepens, the salinity decreases, the water body is diluted, and the concentration of  $\text{CO}_3^{2-}$  and  $\text{Ca}^{2+}$  ions in the water



**FIGURE 12** Governing factors of sedimentary structure

body is reduced, which is not conducive to the preservation of fine microcrystalline carbonate crystal grains. Dissolution often occurs, and the final production is mostly in the form of micrite lamella or micrite.

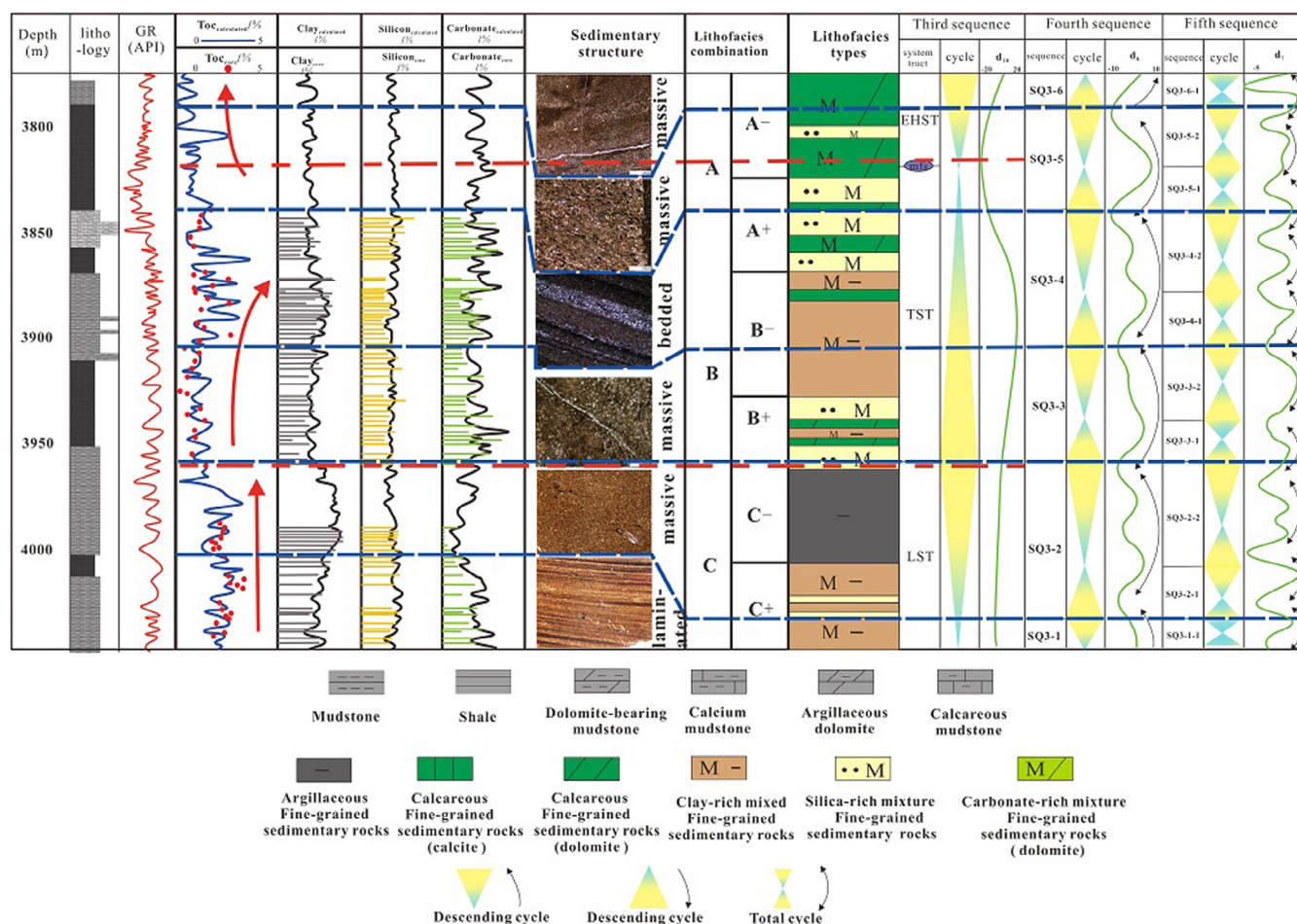
#### 4.5 | Lithofacies combination mode and sedimentary model in high-frequency sequence

The deep lake-semi-deep lake facies sedimentary zone of the second Member of the Funing Formation is far away from the provenance input, and its deposition is controlled by the Mie cycle, showing obvious cyclicity and sequence in the vertical direction (see Figure 13). The TOC change trend is consistent with the third-order sequence change, while the fourth-order sequence controls the vertical combination of fine-grained sedimentary rock facies, and the high-frequency sequence controls the lithofacies type and coupling rhythm changes as a whole. The fine-grained sediments of the second Member of the Funing Formation developed 12 types of lithofacies, showing obvious vertical sequence and cyclicity under the sequence frameworks of different scales, and the overall performance is a tertiary sequence system tract controlling lithofacies types, the four-level sequence controls the lithofacies subtypes and coupled rhythms (Figure 13). According to the lithofacies coupling rhythm in

different system tracts, three lithofacies combinations of A, B, and C are summarized.

A-type lithofacies assemblages are developed in LST. During the deposition of the low-stand system tract, the climate was hot and dry ( $Sr/Cu > 32$ ), evaporation was strong, the lake level was low, and the water body salinity was high ( $Sr/Ba > 1.1$ ). Surface weathering weakened and the supply of terrigenous clastic decreased, forming a lithofacies combination dominated by carbonate-rich mixed fine-grained sedimentary rocks, followed by felsic-rich mixed fine-grained sedimentary rocks. The low system tract is not affected by transgression. The elevation of the lake level is controlled by the fourth-order sequence (long eccentricity cycle), so a warm and humid semi-cycle lithofacies assemblage (A+) and a cold and dry semi-cycle lithofacies assemblage (A-) are formed. The warm and humid semi-cycle rainfall is relatively high, the lake level rises, the average TOC of the lithofacies combination A+ is higher, and the felsic mineral content is high. The sedimentary structure is mainly massive, mainly rich in organic matter in thick layers. Mixed fine-grained sedimentary rocks with thin layers of poor organic matter and massive carbonate-rich mixed fine-grained sedimentary rocks (Figure 12); on the contrary, the cold and dry semi-cycle rainfall is relatively small, the lake level drops, carbonate minerals are precipitated, and they are evaporating A large amount of dolomite is formed in the environment. The lithofacies A- has a low TOC content and a high content of carbonate minerals. The





**FIGURE 13** Distribution of TOC, mineral compositions, and sedimentary structure in high-frequency stratigraphic sequence

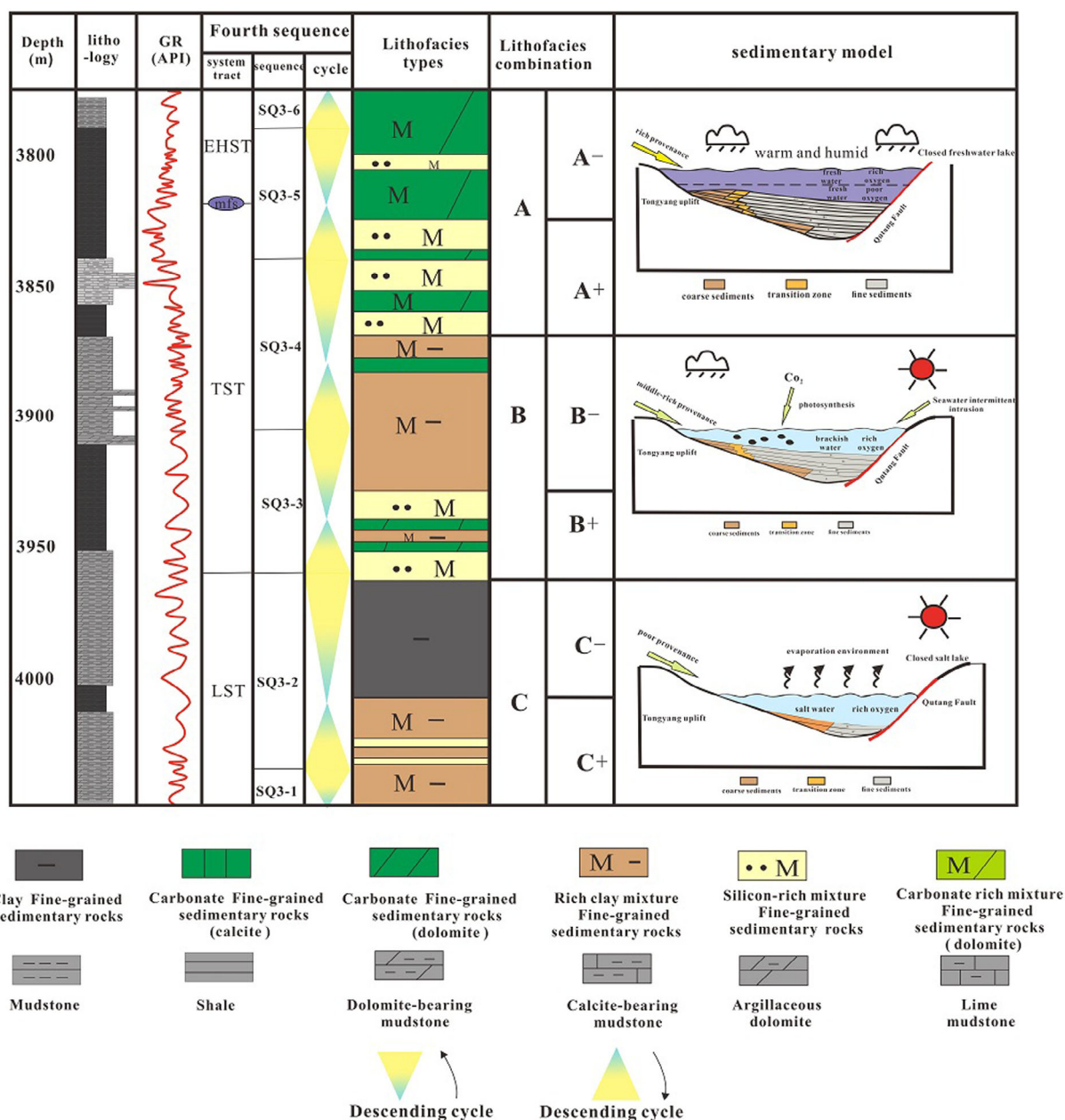
sedimentary structure is mainly massive, mainly thick-layered, organic-poor, massive, carbonate-rich mixed fine-grained sedimentary rocks. The thin layer of organic matter is a massive felsic-rich mixed fine-grained sedimentary rock (Figure 14). There are two cold and dry semi-cycles and one warm and humid semi-cycle developed in the low-stand system tract of the second Member of the Funing Formation, forming a lithofacies depositional model of A—A+—A— (Figure 14).

Type B lithofacies assemblages developed in the TST. During the deposition period of the TST, hot and semi-arid and warm and semi-humid climates alternately appeared, and the overall transition to warm and humid over time (Sr/Cu ranged from 9 to 44, with an average of 21.4), the water body was an oxygen-rich brackish water environment (Sr/Ba is between 0.43 and 1.68, with an average of 0.8). The rainfall is relatively abundant, the intermittent intrusion of seawater causes the lake level to rise rapidly, and the content of TOC and clay minerals shows a rapid upward trend, mainly composed of rich felsic mixed fine particles Sedimentary rock and clay-rich mixed fine-grained sedimentary rock. Affected by the intermittent intrusion of seawater and alternate climate changes, the intermittent sudden increase of palaeo-salinity and the transient growth of organisms will cause the water body to be rich in carbon through photosynthesis,

and some thin-layer carbon will also appear. Salt fine-grained sedimentary rocks. Unlike the low-stand system, the lake level change of the TST is mainly affected by the transgression, and the lake level rises rapidly in the warm and humid semi-circular lake. Layers of organic-poor dolomitic fine-grained sedimentary rocks (Figure 14); the cold and arid semi-circular lake level remains at a higher position or slightly decreases, so the content of calcite in the sedimentary rocks gradually increases, and the layered-lamellar sedimentary structure begins to develop, mainly The medium-organic-rich laminar layered clay-rich mixed fine-grained sedimentary rock and the medium-organic laminar layered grey fine-grained sedimentary rock are thin interbeds (Figure 14). In the second Member of the Funing Formation of the TST, two fourth-order sequences with type B lithofacies developed, forming a lithofacies deposition model of B+—B—B+—B— (Figure 14).

The C-type lithofacies assemblage developed near the largest flooding surface (mfs) and the EHST. Its deposition period was a warm and humid climate (Sr/Cu < 5), with abundant rainfall and sufficient source supply, plus lake water at a stable high-water level, the bottom of the lake Basin is an oxygen-poor reducing environment, which provides good conditions for the preservation of organic matter. The type C lithofacies assemblage is mainly composed of clay-rich mixed fine-





**FIGURE 14** The sedimentary model of the lithofacies assembly

grained sedimentary rocks and clayey fine-grained sedimentary rocks. On the one hand, the warm and humid semi-cycle (C+) has sufficient terrigenous clastic, and the content of felsic and clay minerals increases. On the other hand, palaeontology It flourishes in a warm and humid climate, and the absorption of large amounts of CO<sub>2</sub> leads to an increase in the content of carbonate minerals. Therefore, the content of each mineral is relatively even. The main development of organic-rich laminar layered clay-rich mixed fine-grained sedimentary rocks (Figure 12); Cyclic (C-) source supply decreased, palaeontology decreased, and some felsic minerals transformed into clay minerals, resulting in prominent advantages in clay mineral content, mainly organic-rich massive clayey fine-grained sedimentary rocks (Figure 14). There are two warm and humid semi-cycles and one cold and dry semi-cycle in the second Member of the Funing Formation.

There are two types of C-type lithofacies assemblages, forming a C+—C—C+ lithofacies deposition model (Figure 14).

## 5 | CONCLUSIONS

The second Member of the Funing Formation was divided into the LST and the TST by analysing the characteristics of the logging spectrum curve. (TST) and the EHST, corresponding to 6 four-level sequences and 10 five-level sequences. The E<sub>1</sub>f<sup>2</sup> fine-grained sediments are divided into 12 lithofacies.

The lithofacies type is affected by the palaeoenvironment. The deeper the water body and the hypoxic conditions are the basis for the production and preservation of organic matter; the deeper the

palaeowater body reflects the stronger the weathering of the land surface, which is conducive to the accumulation of clay minerals and felsic minerals. Carbonate deposition is mainly controlled by ancient salinity; anoxic conditions and an increase in ancient salinity are conducive to the development of laminar structures.

The lithofacies of the second Member of the Funing Formation show obvious vertical sequence and cyclicity under the sequence framework of different scales. The third-order sequence system tract controls the organic matter enrichment, and the fourth-order sequence controls the lithofacies subclasses and coupling rhythms. Three lithofacies assemblage models A, B, and C developed in different system tracts were established, and deposition models of different lithofacies assemblage patterns were established based on the results of the palaeoenvironmental analysis.

## ACKNOWLEDGEMENTS

This work was financially supported by the National Natural Science Foundation of China (Grant No. 42072150). We also thank PetroChina Zhejiang Oilfield Company for providing samples and data access.

## CONFLICT OF INTEREST

The authors declare that they have no known competing financial interests or personal relationships that could have appeared to influence the work reported in this paper.

## PEER REVIEW

The peer review history for this article is available at <https://publons.com/publon/10.1002/gj.4526>.

## DATA AVAILABILITY STATEMENT

The data that supports the findings of this study are available in Table 1 and Table 2 of this article.

## REFERENCES

- Aplin, A. C., & Macquaker, J. H. S. (2011). Mudstone diversity: Origin and implications for source, seal, and reservoir properties in petroleum systems. *American Association of Petroleum Geologists Bulletin*, 95, 2031–2059. <https://doi.org/10.1306/03281110162>.
- Bechtel, A., Jia, J., Strobl, S. A. I., Sachsenhofer, R. F., Liu, Z., Gratzner, R., & Püttmann, W. (2012). Palaeoenvironmental conditions during deposition of the Upper Cretaceous oil shale sequences in the Songliao Basin (NE China): Implications from geochemical analysis. *Organic Geochemistry*, 46, 76–95. <https://doi.org/10.1016/j.orggeochem.2012.02.003>.
- Bhattacharya, S., Carr, T. R., & Pal, M. (2016). Comparison of supervised and unsupervised approaches for mudstone lithofacies classification: Case studies from the Bakken and Mahantango-Marcellus Shale, USA. *Journal of Natural Gas Science and Engineering*, 33, 1119–1133. <https://doi.org/10.1016/j.jngse.2016.04.055>.
- Birdwell, J. E., & Washburn, K. E. (2015). Multivariate analysis relating oil shale geochemical properties to NMR relaxometry. *Energy and Fuels*, 29, 2234–2243. <https://doi.org/10.1021/ef502828k>.
- Boucot, A. J., & Gray, J. (2001). A critique of Phanerozoic climatic models involving changes in the CO<sub>2</sub> content of the atmosphere. *Earth-Science Reviews*, 56, 1–159. [https://doi.org/10.1016/S0012-8252\(01\)00066-6](https://doi.org/10.1016/S0012-8252(01)00066-6).
- Cao, B., Xuebin, D. U., Yongchao, L. U., Liu, H., Liu, Z., Yiquan, M. A., ... Peng, L. (2019). Identification and controlling factors of multi-scale lithofacies for continental shale under an isochronous stratigraphic framework: a case study in Dongying Sag, Bohai Bay Basin. *Petroleum Geology Experiment*, 41, 752–759.
- Cather, M., Rose-Coss, D., Gallagher, S., Trujillo, N., Cather, S., Hollingworth, R.S., Mozley, P., Leary, R.J., 2021. Deposition, diagenesis, and sequence stratigraphy of the Pennsylvanian Morrowan and Atokan intervals at Farnsworth unit. *Energies*, 14, 1057. <https://doi.org/10.3390/en14041057>.
- Chen, D., Pang, X., Wang, Y., Dong, Y., Jiang, F., Li, L., ... Jiang, H. (2020). Palaeoenvironmental periodisms of middle Eocene terrestrial sediments in Bohai Bay Basin, eastern China, and their implications for organic matter accumulation. *Marine and Petroleum Geology*, 112, 1–10. <https://doi.org/10.1016/j.marpetgeo.2019.104060>.
- Chen, L., Lu, Y., Jiang, S., Li, J., Guo, T., & Luo, C. (2015). Heterogeneity of the lower Silurian Longmaxi marine shale in the southeast Sichuan Basin of China. *Marine and Petroleum Geology*, 65, 232–246. <https://doi.org/10.1016/j.marpetgeo.2015.04.003>.
- Cheng, Q., Zhang, M., & Li, H. (2019). Anomalous distribution of steranes in deep lacustrine facies low maturity-maturity source rocks and oil of Funing Formation in Subei Basin. *Journal of Petroleum Science and Engineering*, 181, 106190. <https://doi.org/10.1016/j.petrol.2019.106190>.
- Cichon-Pupienis, A., Littke, R., Lazauskienė, J., Baniasad, A., Pupienis, D., Radzevičius, S., & Šiliasauskas, L. (2021). Geochemical and sedimentary facies study – Implication for driving mechanisms of organic matter enrichment in the lower Silurian fine-grained mudstones in the Baltic Basin (W Lithuania). *International Journal of Coal Geology*, 244, 1–24. <https://doi.org/10.1016/j.coal.2021.103815>.
- Dahl, J. E. P., Moldowan, J. M., Teerman, S. C., McCaffrey, M. A., Sundararaman, P., & Stelling, C. E. (1994). Source rock quality determination from oil biomarkers I: A new geochemical technique. *American Association of Petroleum Geologists Bulletin*, 78, 1507–1526. <https://doi.org/10.1306/a25ff201-171b-11d7-8645000102c1865d>.
- Dong, T., Harris, N. B., Ayranci, K., Twemlow, C. E., & Nassichuk, B. R. (2015). Porosity characteristics of the Devonian Horn River shale, Canada: Insights from lithofacies classification and shale composition. *International Journal of Coal Geology*, 141–142, 74–90. <https://doi.org/10.1016/j.coal.2015.03.001>.
- Dymond, J. (1992). Ba as proxy. *Paleoceanography*, 7, 163–181.
- Flemming, B. W. (2000). A revised textural classification of gravel-free muddy sediments on the basis of ternary diagrams. *Continental Shelf Research*, 20, 1125–1137. [https://doi.org/10.1016/S0278-4343\(00\)00015-7](https://doi.org/10.1016/S0278-4343(00)00015-7).
- Fu, Q., Li, Y., Zhang, G., & Liu, Y. (2008). Evidence of the transgression lake of the Subei Basin during Late Cretaceous and Paleocene and its geological significance. *Frontiers of Earth Science in China*, 2, 114–119. <https://doi.org/10.1007/s11707-008-0004-2>.
- Hemmesch, N. T., Harris, N. B., Mnich, C. A., & Selby, D. (2014). A sequence-stratigraphic framework for the Upper Devonian Woodford Shale, Permian Basin, west Texas. *American Association of Petroleum Geologists Bulletin*, 98, 23–47.
- Hickey, J. J., & Henk, B. (2007). Lithofacies summary of the Mississippian Barnett Shale, Mitchell 2 T.P. Sims well, Wise County, Texas. *American Association of Petroleum Geologists Bulletin*, 91, 437–443. <https://doi.org/10.1306/12040606053>.
- Hu, W., Ma, L., Liu, Y., Li, Y., Xin, C., Liu, X., ... Ma, L. (2018). Geochemical characteristics of hydrocarbon source rocks in Fu2 member of Qutang subsag, Haian sag, Subei Basin. *Journal of Northeast Petroleum University*, 42, 73–81.
- Ibad, S. M., & Padmanabhan, E. (2022). Lithofacies, mineralogy, and pore types in Paleozoic gas shales from Western Peninsular Malaysia. *Journal of Petroleum Science and Engineering*, 212, 110239. <https://doi.org/10.1016/j.petrol.2022.110239>.
- Jarvis, I., Murphy, A. M., & Gale, A. S. (2001). Geochemistry of pelagic and hemipelagic carbonates: Criteria for identifying systems tracts and

- sea-level change. *Journal of the Geological Society of London*, 158, 685–696. <https://doi.org/10.1144/jgs.158.4.685>.
- Jones, B., & Manning, D. A. C. (1994). Comparison of geochemical indices used for the interpretation of palaeoredox conditions in ancient mudstones. *Chemical Geology*, 111, 111–129. [https://doi.org/10.1016/0009-2541\(94\)90085-X](https://doi.org/10.1016/0009-2541(94)90085-X).
- Kadhodaie, A., & Rezaee, R. (2017). Intelligent sequence stratigraphy through a wavelet-based decomposition of well log data. *Journal of Natural Gas Science and Engineering*, 40, 38–50. <https://doi.org/10.1016/j.jngse.2017.02.010>.
- Kai-xun, Z., Guoping, B., Quan, W., Xinjie, N., Qiuwei, L., & Xiaoxin, L. (2016). Wireline log response-based recognition and evaluation of diagenetic facies in tight sandstone reservoirs: A case study of the Member 3 of Paleogene Shahejie Formation in Raoyang sag of Jizhong Depression. *Journal of Palaeogeography*, 18, 921–938.
- Khalifa, M. A. (2005). Lithofacies, diagenesis and cyclicity of the “Lower Member” of the Khuff Formation (Late Permian), Al Qasim Province, Saudi Arabia. *Journal of Asian Earth Sciences*, 25, 719–734. <https://doi.org/10.1016/j.jseae.2004.05.008>.
- Lapidus, A. L., Kerimov, V. Y., Mustaev, R. N., Movsumzade, E. M., & Zakharchenko, M. V. (2018). Caucasus Maykopian kerogenous shale sequences: Generative potential. *Oil Shale*, 35, 113–127. <https://doi.org/10.3176/oil.2018.2.02>.
- Leven, E. J. (2013). Stratigraphy of the Carboniferous-Permian volcanosedimentary sequences of the Northern Pamir, Tajikistan. *Stratigraphy and Geological Correlation*, 21, 601–608. <https://doi.org/10.1134/S0869593813060063>.
- Li, Z., & Schieber, J. (2018). Detailed facies analysis of the Upper Cretaceous Tununk Shale Member, Henry Mountains Region, Utah: Implications for mudstone depositional models in epicontinental seas. *Sedimentary Geology*, 364, 141–159. <https://doi.org/10.1016/j.sedgeo.2017.12.015>.
- Liu, B., Song, Y., Zhu, K., Su, P., Ye, X., & Zhao, W. (2020). Mineralogy and element geochemistry of salinized lacustrine organic-rich shale in the Middle Permian Santanghu Basin: Implications for paleoenvironment, provenance, tectonic setting and shale oil potential. *Marine and Petroleum Geology*, 120, 104569. <https://doi.org/10.1016/j.marpetgeo.2020.104569>.
- Liu, X., Lai, J., Fan, X., Shu, H., Wang, G., Ma, X., ... Luo, Y. (2020). Insights in the pore structure, fluid mobility and oiliness in oil shales of Paleogene Funing Formation in Subei Basin, China. *Marine and Petroleum Geology*, 114, 104228. <https://doi.org/10.1016/j.marpetgeo.2020.104228>.
- Loucks, R. G., & Ruppel, S. C. (2007). Mississippian Barnett Shale: Lithofacies and depositional setting of a deep-water shale-gas succession in the Fort Worth Basin, Texas. *American Association of Petroleum Geologists Bulletin*, 91, 579–601. <https://doi.org/10.1306/11020606059>.
- Mussa, A., Kalkreuth, W., Pimentel Mizusaki, A. M., & Bicca, M. M. (2021). Geochemical characterization of selected organic-rich shales from the Devonian Pimenteiras Formation, Parnaíba Basin, Brazil – Implications for methane adsorption capacity. *Journal of South American Earth Sciences*, 112, 103507. <https://doi.org/10.1016/j.jsames.2021.103507>.
- Nwaezeapu, V. C., Okoro, A. U., Akpunonu, E. O., Ajaegwu, N. E., Ezenwaka, K. C., & Ahaneke, C. V. (2018). Sequence stratigraphic approach to hydrocarbon exploration: a case study of Chiadu field at eastern onshore Niger Delta Basin, Nigeria. *Journal of Petroleum Exploration and Production Technology*, 8, 399–415. <https://doi.org/10.1007/s13202-017-0405-4>.
- Olsen, P. E., & Whiteside, J. H. (2009). Pre-Quaternary Milankovitch Cycles and Climate Variability. In: V. Gornitz (Ed.), *Encyclopedia of Paleoclimatology and Ancient Environments*. Springer, Dordrecht: Encyclopedia of Earth Sciences Series. [https://doi.org/10.1007/978-1-4020-4411-3\\_195](https://doi.org/10.1007/978-1-4020-4411-3_195).
- Pepper, A. S., & Corvi, P. J. (1995). Simple kinetic models of petroleum formation. Part I: oil and gas generation from kerogen. *Marine and Petroleum Geology*, 12, 291–319. [https://doi.org/10.1016/0264-8172\(95\)98381-E](https://doi.org/10.1016/0264-8172(95)98381-E).
- Ross, D. J. K., & Bustin, R. M. (2008). Characterizing the shale gas resource potential of Devonian-Mississippian strata in the Western Canada sedimentary Basin: Application of an integrated formation evaluation. *American Association of Petroleum Geologists Bulletin*, 92, 87–125. <https://doi.org/10.1306/09040707048>.
- Shi, J., Jin, Z., Liu, Q., & Huang, Z. (2020). Depositional process and astronomical forcing model of lacustrine fine-grained sedimentary rocks: A case study of the Early Paleogene in the Dongying Sag, Bohai Bay Basin. *Marine and Petroleum Geology*, 113, 103995. <https://doi.org/10.1016/j.marpetgeo.2019.08.023>.
- Shi, J., Jin, Z., Liu, Q., Zhang, R., & Huang, Z. (2019). Cyclostratigraphy and astronomical tuning of the middle eocene terrestrial successions in the Bohai Bay Basin, Eastern China. *Global and Planetary Change*, 174, 115–126. <https://doi.org/10.1016/j.gloplacha.2019.01.001>.
- Trabucho-Alexandre, J., Dirkx, R., Veld, H., Klaver, G., & De Boer, P. L. (2012). Toarcian black shales in the dutch central graben: Record of energetic, variable depositional conditions during an oceanic anoxic event. *Journal of Sedimentary Research*, 82, 104–120. <https://doi.org/10.2110/jsr.2012.5>.
- Tucker, M., & Garland, J. (2010). High-frequency cycles and their sequence stratigraphic context: Orbital forcing and tectonic controls on Devonian cyclicity, Belgium. *Geologica Belgica*, 13, 213–240.
- Wang, Y., & Chen, Y. (1992). A discussion of the palaeogene transgression in north Jiangsu Basin. *Acta Pharmaceutica Sinica*, 13, 137–142.
- Wang, Y., Wang, X. J., Song, G. Q., Liu, H. M., Zhu, D. S., Zhu, D. Y., Ding, J. H. ... Wang M. (2016). Genetic connection between mud shale lithofacies and shale oil enrichment in jiyang depression, bohai bay basin. *Petroleum Exploration and Development*, 43(5), 696–704.
- Wei, X. F., Zhang, T. S., Liang, X., Yao, Q. C., & Tang, X. Y. (2012). Sequence stratigraphy and sedimentary characteristics of taizhou Formation in baiju sag. *Geology in China*, 39, 400–413.
- Xuebin, D. U., Yongchao, L. U., Liu, H., Liu, H., Wang, Y., Xiong, S., ... Peng, L. (2018). Division of high-frequency sequences of different orders in fine-grained deposits and its geologic significance: A case study of mud shale from the lower section of the third member to the upper section of the fourth member of Shahejie Formation in Dongyin. *Petroleum Geology Experiment*, 40, 244–252.
- Yang, W., Zuo, R., Chen, D., Jiang, Z., Guo, L., Liu, Z., ... Zhang, C. (2019). Climate and tectonic-driven deposition of sandwiched continental shale units: New insights from petrology, geochemistry, and integrated provenance analyses (the western Sichuan subsiding Basin, Southwest China). *International Journal of Coal Geology*, 211, 103227. <https://doi.org/10.1016/j.coal.2019.103227>.
- Zhang, K., Bai, G., Jin, F., & Wang, Q. (2016). Diagenesis in sequence stratigraphical framework: a case study of sandstone of Member 3 of Shahejie Formation in the south-central Raoyang sag. *Acta Petrolei Sinica*, 37, 728–742. <https://doi.org/10.7623/syxb201606004>.
- Zhang, M., & Li, Z. (2018). The lithofacies and reservoir characteristics of the fine-grained sedimentary rocks of the Permian Lucaogou Formation at the northern foot of Bogda Mountains, Junggar Basin (NW China). *Journal of Petroleum Science and Engineering*, 170, 21–39. <https://doi.org/10.1016/j.petrol.2018.06.007>.
- Zhu, J., Jiang, X., Xu, X., & Zhang, Y. (2005). The cenozoic evolution and petroleum response estimation in the qutang-libao region of the haian depression, the north Jiangsu Basin. *Petroleum Geology Experiment*, 27, 138–143.

**How to cite this article:** Sun, B., Liu, X., Liu, J., Wang, G., Shu, H., Luo, Y., Liu, T., & Hua, Z. (2022). The heterogeneity of lithofacies types, combination modes, and sedimentary model of lacustrine shale restricted by high-frequency sequence. *Geological Journal*, 1–17. <https://doi.org/10.1002/gj.4526>